

# Hydrodynamics and Oxygen Transfer in Pneumatic Bioreactor Devices

M. Y. Chisti and M. Moo-Young

Department of Chemical Engineering, University of Waterloo, Waterloo, Ontario, Canada N2L 3G1

Accepted for publication March 24, 1987

Gas holdup and oxygen transfer studies in non-Newtonian suspensions of cellulose fibres conducted in two large (0.098 m<sup>3</sup> each) reactors are described. Both reactors—a bubble column and a similar internal loop airlift—were unusual in that they had rectangular cross-sections. In all cases gas holdups and  $k_L a_L$  declined with increasing solid concentration and, under identical conditions, the bubble column performed better than the airlift. The fluid systems used were carefully selected to represent mould fermentation broths. The behavior of true mass transfer coefficient  $k_L$  with changes in bubble size is discussed for these systems.

## INTRODUCTION

Despite many advantages, the commercial application of pneumatically agitated reactors in biotechnology is still quite limited due to insufficient data available for their design. Even for circular bubble columns which are the most thoroughly investigated design among the newer reactors, most of the work has been in water or waterlike fluids which do not simulate the media encountered in fungal fermentations even remotely.

A few studies of bubble columns<sup>1-6</sup> and airlift towers<sup>7,8</sup> in non-Newtonian polymer solutions exist. These fluids, while a suitable representation of certain fermentation systems, are unsatisfactory for the duplication of mycelial broths. Homogeneous polymer solutions such as those of carboxymethyl cellulose (CMC) commonly follow the power-law behavior with the flow index ( $n$ ) and consistency index ( $K$ ) dependent on the concentration of the dissolved polymer, as shown in Figure 1, which is typical. Independent variation of  $K$  and  $n$  in polymer solutions is difficult and in order to obtain low  $n$  values the polymer concentrations necessary are such that quite high  $K$  values result. Fungal systems, on the other hand, not only have low  $n$ , but  $K$  values are also relatively low. For example, for *Aspergillus niger* suspensions (2–10 kg/m<sup>3</sup> dry biomass)  $n$  was reported<sup>9</sup> to vary from ca. 0.6 to 0.16 whereas  $K$  increased from 0.17 Pa s<sup>0.6</sup> to 9.1 Pa s<sup>0.16</sup>. In addition, the microturbulence characteristics in homogeneous media are expected to be different than in systems containing suspended solids.

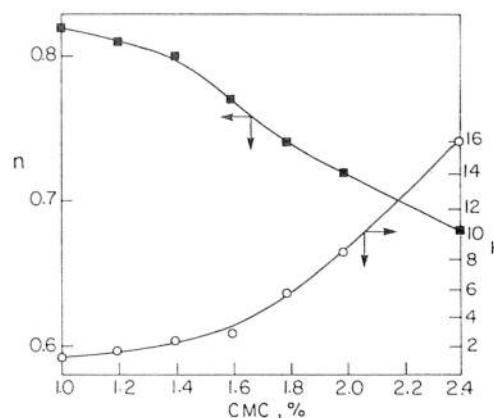


Figure 1. Consistency index  $K$  and flow behavior index  $n$  as a function of CMC concentration (from ref. 1).

On the basis of foregoing considerations and with the aim of examining the hydrodynamic and mass transfer properties of pneumatic reactors for application to mould fermentations such as those of *Aspergillus*, *Penicillium* and *Chaetomium*, we studied gas-liquid-solid model systems in a bubble column and in an internal loop airlift tower, both with an unusual rectangular geometry. This work is described in the following sections.

## THEORY

The liquid film control of mass transfer of a sparingly soluble gas from the gas to the liquid phase is well known and the transport rate is given by:

$$\frac{dC_L}{dt} = k_L a_L (C^* - C_L) \quad (1)$$

where  $k_L a_L$ ,  $C^*$  and  $C_L$  are the overall volumetric mass transfer coefficient, the saturation concentration of oxygen in the liquid and the liquid phase oxygen concentration at any time,  $t$ , respectively. Integration of eq. (1) between the limits  $C_L = C_0$  at  $t = 0$ , and  $C_L = C_L$  at  $t = t$  yields:

$$\ln \frac{(C^* - C_0)}{(C^* - C_L)} = k_L a_L t \quad (2)$$

which may be utilized for  $k_L a_L$  determination based on the transient gassing-in method. For point measurements, eq. (2) is valid only when the reactor is fully backmixed.

In the transient technique the dynamics of the oxygen electrode itself influence  $k_L a_L$  results. The electrode delays which are a function of fluid hydrodynamics near its measuring surface may be satisfactorily accounted for by the first-order model<sup>3,10</sup>:

$$\frac{(C^* - C_L)}{(C^* - C_0)} = \left( \frac{e^{-t/B} - e^{-t/S}}{B - S} \right) \frac{BS}{(B - S)} \quad (3)$$

where  $S$  and  $B$  are the electrode time lag and the reciprocal of  $k_L a_L$ , respectively. For  $t \gg S$ , eq. (3) reduces to:

$$\frac{(C^* - C_L)}{(C^* - C_0)} = \frac{B e^{-t/B}}{(B - S)} \quad (4)$$

A semilog plot of  $(C^* - C_L)/(C^* - C_0)$  vs.  $t$  would yield a straight line of slope  $-1/B$  (or  $-k_L a_L$ ) and intercept  $\ln[B/(B - S)]$  from which the time delay may be obtained.

Apart from  $k_L a_L$  the other important parameter in bio-reactor design is the fractional gas holdup,  $\epsilon$ . The residence time ( $t_G$ ) of the gas in liquid, the gas-liquid interfacial area for mass transfer ( $a_L$ ) and, in airlifts, the circulation of liquid, all depend on gas holdup:

$$a_L = \frac{6}{d_B} \frac{\epsilon}{(1 - \epsilon)} \quad (5)$$

and

$$t_G = \left( \frac{V_L}{Q_G} \right) \frac{\epsilon}{(1 - \epsilon)} \quad (6)$$

Multiplying eq. (5) by the true mass transfer coefficient,  $k_L$ , we obtain:

$$k_L a_L = \frac{6k_L}{d_B} \frac{\epsilon}{(1 - \epsilon)} \quad (7)$$

and taking logarithms, we get:

$$\ln k_L a_L = \ln \left( \frac{6k_L}{d_B} \right) + \ln \frac{\epsilon}{(1 - \epsilon)} \quad (8)$$

This is an important, purely theoretically derived, relationship and it suggests that a log-log plot of  $k_L a_L$  vs.  $\epsilon/(1 - \epsilon)$  should have unit slope. Also eq. (7) may be rearranged to give:

$$\frac{k_L}{d_B} = \frac{k_L a_L (1 - \epsilon)}{6\epsilon} \quad (9)$$

Using the easily measured overall volumetric mass transfer coefficient ( $k_L a_L$ ) and gas holdup ( $\epsilon$ ) in eq. (9) it becomes possible to calculate the ratio  $k_L/d_B$  the behavior of which will be shown to be helpful in understanding the mass transfer phenomena. Since direct experimental measurements of  $a_L$  are more difficult and less reliable, the  $k_L$  calculated from measured  $k_L a_L$  and experimentally obtained  $a_L$  has frequently led to contradictory results in earlier investigations. For example,  $k_L$  relationships have often shown it to vary

with the bubble diameter according to  $d_B^m$  where  $m$  has been variously quoted as 0.5,<sup>11</sup>  $-0.25$ ,<sup>12</sup>  $-0.4$ ,<sup>13</sup> and 0.891.<sup>14</sup> Despite its simplicity, we have not come across any reports interpreting  $k_L a_L$  and gas holdup in the way that eq. (9) does.

## Experimental

A bubble column of rectangular cross section and an airlift tower of similar geometry were used. The relevant dimensions of these are shown in Figure 2. Both vessels were made of transparent perspex and unaerated liquid volumes and liquid heights in them were kept at 0.098 m<sup>3</sup> and 1.372 m, respectively. The bubble column was sparged by a perforated plate (50 holes of 0.001-m diameter) located at its base, while similar spargers (20 holes each, 0.001m diameter) positioned at the bottom of each riser were utilized in the airlift. A plastic prism (Fig. 2) placed just below the downcomer in the airlift ensured a smooth change in flow direction of the fluid exiting the downcomer thereby minimizing energy losses.

Air at 20°C metered via a calibrated rotameter (Schutte and Koerting, 3-HCFB tube, J-type float) was employed for gassing. All the airflow data presented here is at normal temperature and pressure (NTP) and the superficial velocities are based either on the bubble column cross-sectional area or on riser cross section (in airlift). Superficial air velocities ranged from 0 to ca. 0.3 m/s.

Batch liquids or slurries were used throughout, and these included hard tap water, 0.15 kmol/m<sup>3</sup> NaCl solution in tap

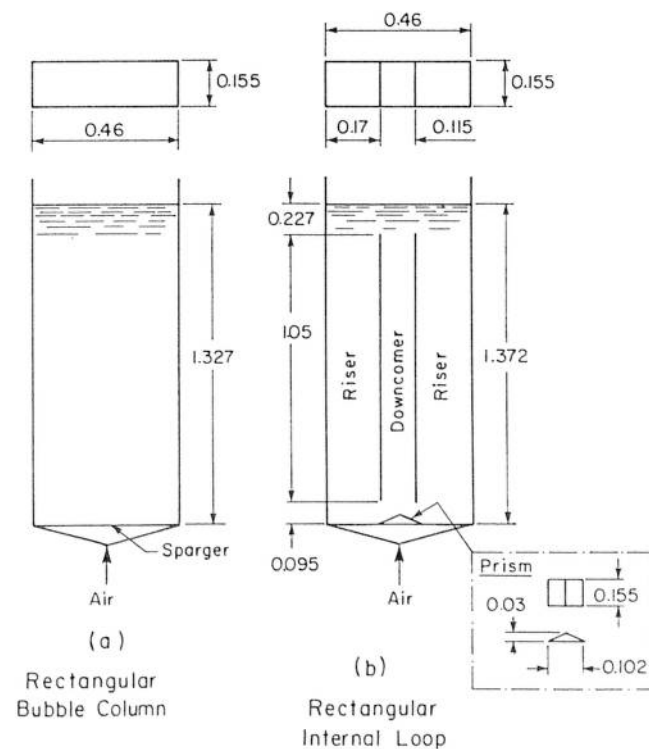


Figure 2. Dimensions of reactors used: (a) rectangular bubble column and (b) rectangular internal loop airlift. All dimensions are in meters (not drawn to scale).

water, 1, 2, and 3% (w/v) suspensions of Solka Floc cellulose fiber grade KS-1016 (James River Corporation) in 0.15 kmol/m<sup>3</sup> NaCl solutions. The properties of Solka Floc are presented in Table I.

The gas holdups were determined either by volume expansion or by manometric measurements of hydrostatic pressure and both techniques were found to be strictly comparable.

The overall volumetric oxygen transfer coefficient,  $k_L a_L$ , was determined by the dynamic gassing-in method using a fast response dissolved oxygen electrode (Yellow Springs, YSI 5739 with Standard membrane) connected to a YSI model 57 dissolved oxygen meter. A constant gas phase composition and a well mixed liquid (or slurry) phase were assumed. The former assumption is well known and the latter was justified because the dissolved oxygen measurements from several different locations in the reactors showed no significant differences. The electrode response displayed a first-order behavior as observed in the past by others.<sup>3,10</sup> However, the  $k_L a_L$  values calculated with electrode delay taken into account and those obtained by ignoring the time lag did not differ by more than 3% in the extreme cases and in subsequent work the electrode dynamics were neglected.

## RESULTS AND DISCUSSION

Solka Floc (SF) suspensions showed a strong resemblance to mycelial fermentation systems such as those of *Aspergillus* and *Penicillium* where pulp form of morphology occurs. Not only was the SF particle size in a range which is typical for moulds (i.e., 200–300  $\mu\text{m}$ ), but also the particle shape which was long thread-like was a close replica of mould mycelia. Moreover, the SF particles were quite flexible and in suspension contained a high proportion of absorbed water. The feel, texture and visual appearance of these suspensions also corresponded to those of fungal broths. In addition, as shown in Table II, the SF suspensions

**Table I.** Properties of Solka Floc (KS-1016).

Average fiber length ( $\mu\text{m}$ )	290
Screen analysis	
Percent on 35 mesh (%)	10.22
Percent through 100 mesh (%)	38.52
Percent through 200 mesh (%)	17.29
Bulk density ( $\text{kg}/\text{m}^3$ )	18.31
Maximum apparent density ( $\text{kg}/\text{m}^3$ )	190
Minimum apparent density ( $\text{kg}/\text{m}^3$ )	50

**Table II.** Comparison of consistency and flow behavior indices of Solka Floc suspensions and *Aspergillus niger* broths.

Dry solid content ( $\text{kg}/\text{m}^3$ )	$n$	$K$ ( $\text{Pa s}^n$ )
2	0.55	0.17
5(20) <sup>a</sup>	0.33(0.322)	1.62(1.464)
10(30)	0.2 (0.237)	9.06(6.127)

<sup>a</sup> The data in parentheses are for the SF suspensions used in this work. The rest of the data is for the *A. niger* broths of ref. 9. The impeller method described in ref. 9 was used for the determination of  $K$  and  $n$  in both cases.

reproduced the  $K$  and  $n$  values of mycelia-containing fluids exceedingly well.

The variation of gas holdup with superficial gas velocity in the bubble column followed the pattern depicted in Figure 3. The initial rapid rise of holdup quickly gave way to a more gradual increase due to greater bubble coalescence originating from a higher bubble collision frequency as the number of bubbles per unit volume became large. Similar results have been reported in homogeneous fluids in the past. The data of Figure 3 replotted on log–log axes in Figure 4 clearly revealed a discontinuity near superficial gas velocities of ca. 0.06 m/s. This corresponded to a visually observed change in flow regime from the bubble to churn-turbulent flow. In either flow regime, the addition of solids (SF) up to 1% (w/v) dry matter did not influence the gas holdup to any

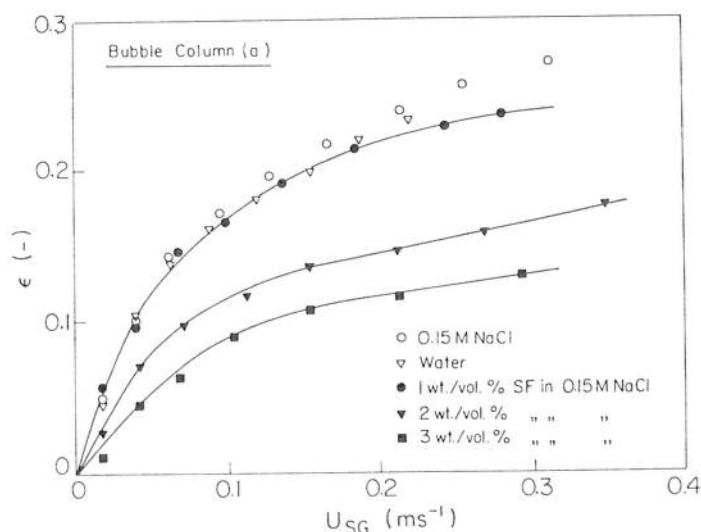


**Figure 3.** Variation of gas holdup with superficial gas velocity in the bubble column. Lines drawn through Solka Floc data.

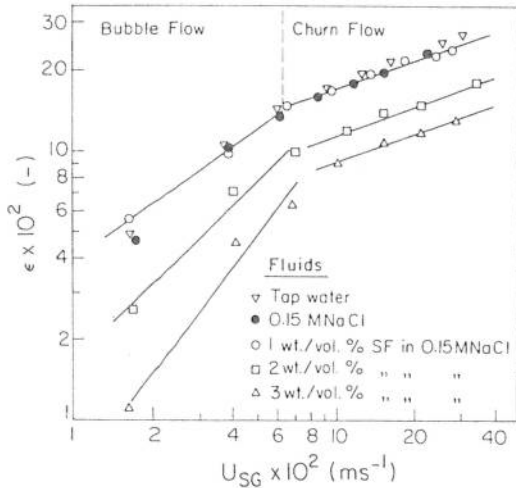


Figure 4. Gas holdup in bubble column. The lines shown are for SF suspensions.

significant degree (Fig. 4); however, with further increase in SF concentration the holdup declined by up to 80%. This may be explained thus: in solid-free aqueous systems of the type used, the scale of Kolmogoroff's terminal eddies can be shown to be between 20 and 40  $\mu\text{m}$ ; the addition of solids, the particle size of which was substantially greater than the scale of terminal eddies, led to damping of turbulence due to drag and hence the reduction in holdup.

The data in Figure 4 are plotted according to the equation:

$$\epsilon = \alpha U_{sg}^{\beta} \quad (10)$$

The values of  $\alpha$  and  $\beta$  for various fluids and flow regimes are summarized in Table III from which several interesting phenomena could be inferred. In the bubble flow region ( $0.015 \leq U_{sg} < 0.07$  m/s), the dependence of gas holdup on superficial gas velocity increased with solid contents between 1 and 3% (w/v), i.e.  $\beta_1$ , increased. In the churn-turbulent regime ( $0.07 \leq U_{sg} < 0.4$  m/s), on the other hand, the exponent ( $\beta_2$ ) on gas velocity was nearly constant irrespective of the solid content of the fluid. This was because the apparent viscosity of these strongly shear thinning suspensions fell rapidly with rising shear rates as the gas velocity increased in the bubble flow regime; consequently, a more rapid increase in turbulence and, therefore in gas holdup, was obtained with increasing gas input in fluids

Table III.  $\alpha$  and  $\beta$  in eq. (10) for the rectangular bubble column.

Fluid [%(w/v) Solka Floc in 0.15M NaCl]	Bubble flow		Churn-turbulent flow		
	$\alpha_1$	$\beta_1$	$\alpha_2$	$\beta_2$	$\beta_1/\beta_2$
0	1.481	0.826	0.441	0.398	2.08
1	0.913	0.683	0.372	0.341	2.00
2	1.269	0.943	0.259	0.363	2.6
3	2.14	1.268	0.200	0.345	3.68

Note: Subscripts 1 and 2 in  $\alpha$  and  $\beta$  refer to bubble flow and churn-turbulent flow, respectively.

which were more shear thinning (i.e., had a greater SF content). In the churn-turbulent regime, however, the gas flow rates and, hence the shear rates in the reactors, were so high that the fluid had already reached the lower limit of its apparent viscosity. Further viscosity changes, if any, were small and the fluid behaved largely as a Newtonian liquid. In such high turbulence fields viscous effects are expected to be small. Consequently,  $\beta_2$  was approximately constant for all fluids. The ratio  $\beta_1/\beta_2$  is an additional indicator of the fact that the greater the shear thinning nature (i.e., the higher the solid content) of the fluid the stronger the gas velocity dependence of holdup in the bubble flow regime relative to churn-turbulent flow.

While the form of eq. (10) is useful for a discussion of the holdup results, a single dimensionless equation which fits all data would be more appropriate. Considering this, all the gas holdup data in water, 0.15M NaCl and in suspensions in the rectangular bubble column in churn-turbulent regime was correlated by the equation:

$$\epsilon = 1.16e^{-(0.273C+0.782)} Fr^{0.362} \quad (11)$$

As shown in Figure 5, eq. (11) fits the data within ca. 10%. The Froude number in eq. (11) is defined as:

$$Fr = \frac{U_{sg}}{(gd_c)^{1/2}} \quad (12)$$

where  $d_c$  is the equivalent diameter of the rectangular bubble column. Although the column diameter was not varied, eq. (11) predicts a  $d_c^{-0.181}$  dependence of holdup on diameter. This is quite reasonable and small decline in gas holdups with increasing column diameters have been frequently observed by other investigators.

In the bubble flow regime the holdup data obtained in the bubble column could not be correlated by a single equation. Correlation (10), with  $\alpha$  and  $\beta$  being 1.481 and 0.826,

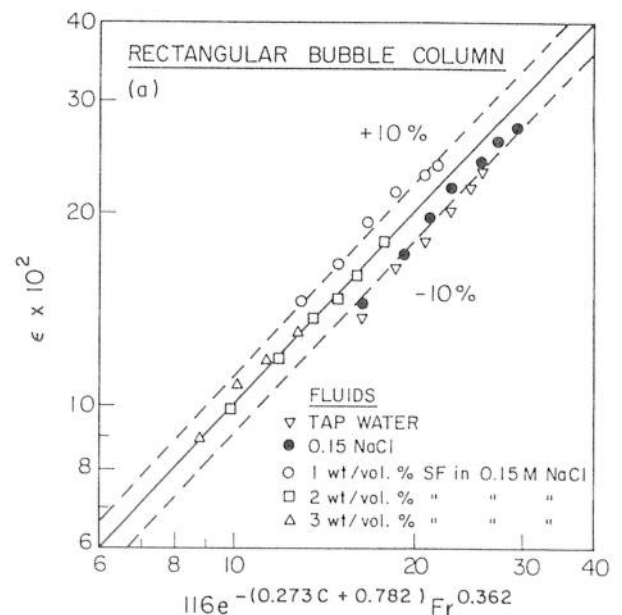


Figure 5. Gas holdup in bubble column in the churn-turbulent regime according to eq. (11). The symbols have the same meanings as in Figure 4.

respectively, applied to 0.15M NaCl solution. For SF suspensions another equation was obtained:

$$\epsilon = U_{sg}^{(0.293C+0.38)} e^{(0.426C-0.549)} \quad (13)$$

which fitted the data within ca.  $\pm 10\%$  (Fig. 6).

The gas holdup variation with gas velocity in the airlift reactor followed the same general pattern as in the bubble column (Fig. 7). Once again, a definite decline in gas holdup with increasing concentration of solids and the flow regime transition were noticed (Fig. 8). Interestingly, the flow regime change from bubble to churn-turbulent flow occurred in a narrow range of superficial gas velocities ( $U_{sg} \approx 0.06-0.07\text{m/s}$ ) which was common to the two reactors used. Under otherwise identical conditions, the gas holdup in the airlift was significantly lower than in the bubble column. This was almost certainly due to high liquid circulation velocities in the airlift reactor which led to an enhancement of bubble rise velocities and hence lower holdups.

The overall volumetric mass transfer coefficient,  $k_L a_L$ , displayed similar behavior in the two reactors as did the gas

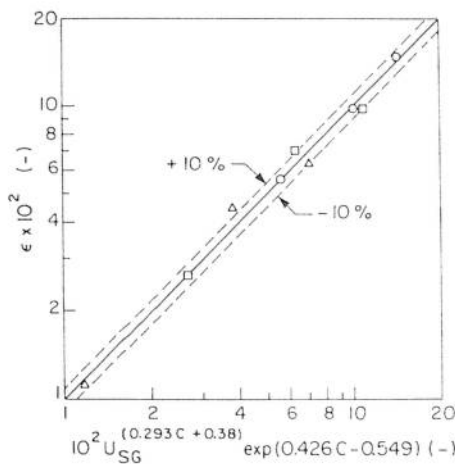


Figure 6. Gas holdup in SF suspension in bubble column in the bubble flow regime according to eq. (13). The symbols have the same meanings as in Figure 4.

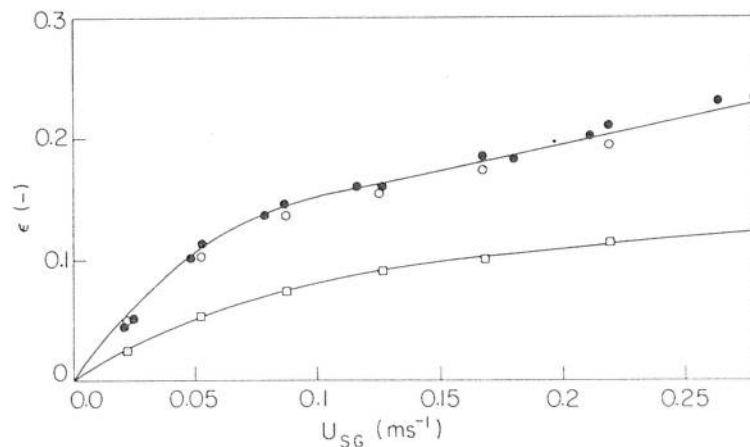


Figure 7. Gas holdup vs. superficial gas velocity in the rectangular airlift. See Figure 4 for an explanation of symbols.

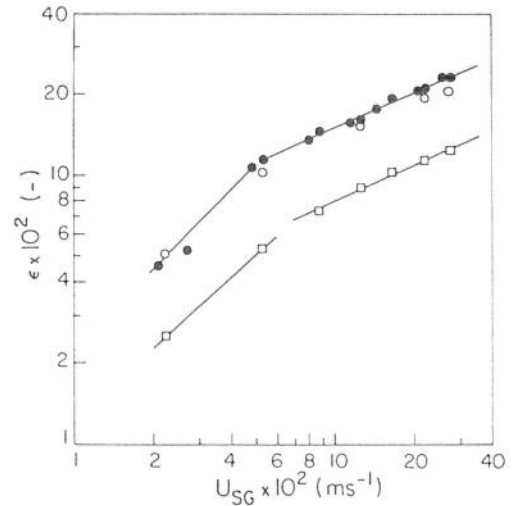


Figure 8. Gas holdup variation with superficial gas velocity in the rectangular airlift: influence of solids and flow regime transition. (Same data are used as in Fig. 7.) See Figure 4 for an explanation of symbols.

holdup. There were differences, however. In the bubble column,  $k_L a_L$  declined with increasing solid content (Fig. 9). The data obtained in 0.15M NaCl solution showed satisfactory order of magnitude agreement with the correlation recommended by Shah<sup>15</sup> (Fig. 9) for circular bubble columns. For suspensions in the bubble column, the following equation was obtained:

$$k_L a_L = (0.317 \pm 0.047) C^{-(1.781 \pm 0.183)} U_{sg}^{(0.637 \pm 0.114)} \quad (14)$$

Equation (14) was applicable to suspensions only [ $C = 1-3\%$  (w/v)] for  $0.016 \leq U_{sg} \leq 0.35$  m/s and it correlated the data within about 20% (Fig. 10). Attempts to fit a single equation to the data obtained in slurries and that from solid free liquids proved unsuccessful probably because of the very different characteristics of those fluids.

A comparison of Figures 4 and 9 shows that the clear breaks which occur in the holdup data at the points of flow transition are not quite so prominent in the  $k_L a_L$  results. While this may seem puzzling it is easily explained by the fact that flow transition is accompanied by changes in

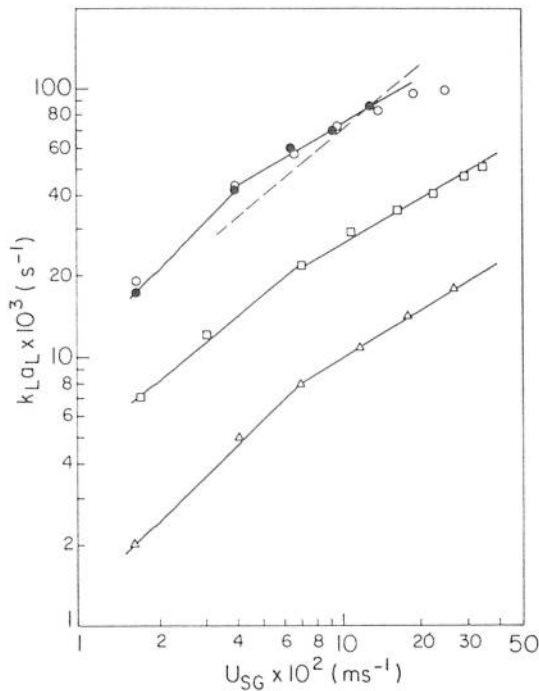


**Figure 9.** Overall volumetric oxygen transfer coefficient vs. superficial gas velocity in the rectangular bubble column. The dashed line represents the correlation of ref. 15:  $k_L a_L (s^{-1}) = 0.467 U_{SG}^{0.82} (m/s)$ . For an explanation of the other symbols, see Figure 4.

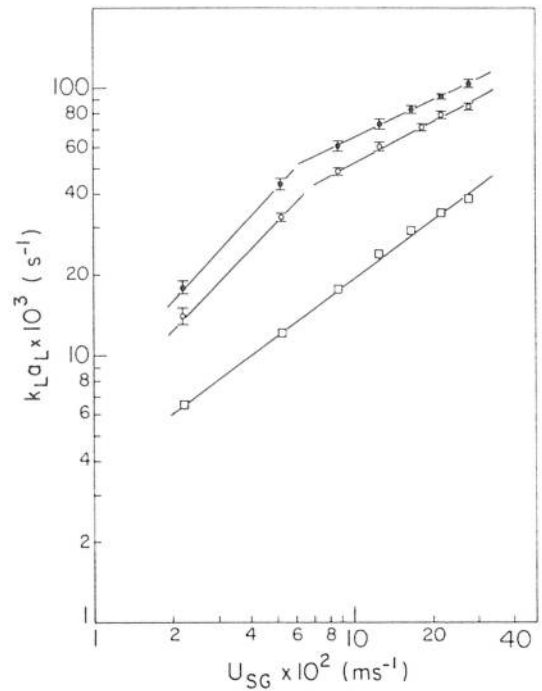


**Figure 11.** Oxygen transfer coefficient vs. superficial gas velocity in the rectangular airlift. The vertical bars represent the spread of the data. All symbols are explained in Figure 4.

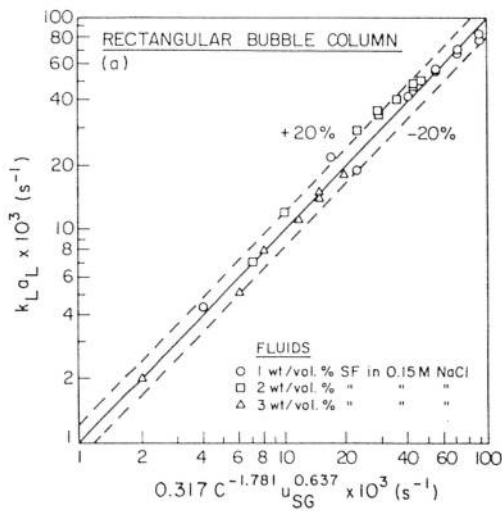


**Figure 10.** Overall volumetric oxygen transfer coefficient in SF suspensions in the rectangular bubble column according to eq. (14). See Figure 4 for an explanation of the symbols.

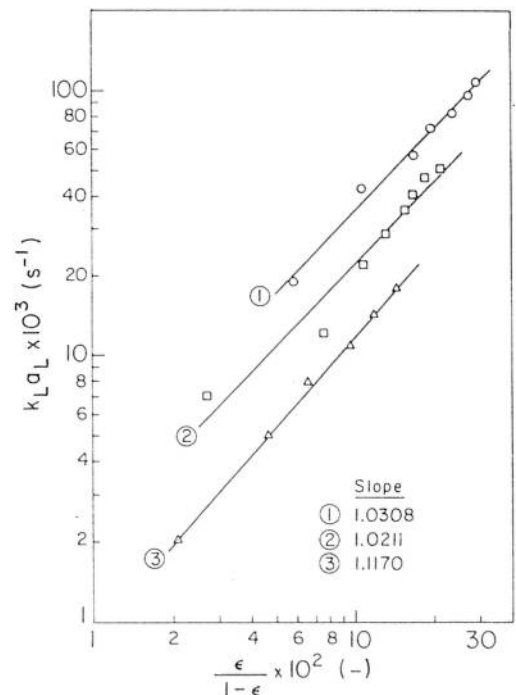


**Figure 12.**  $k_L a_L$  vs.  $\epsilon / (1 - \epsilon)$  in the rectangular bubble column. See Figure 4 for an explanation of the symbols.

bubble size and gas holdup is a stronger function of the bubble diameter than is the interfacial area  $a_L$  in  $k_L a_L$ . Typical  $k_L a_L$  data for the airlift is shown in Figure 11. Comparison of Figures 9 and 11 indicates that under otherwise identical conditions the  $k_L a_L$  in the airlift is up to 40% lower than in the bubble column.

The  $k_L a_L$  and gas holdup data plotted according to eq. (8) is shown in Figures 12 and 13. As expected from theoretical reasoning, these plots do indeed have a unit slope irrespective of the reactor type and the prevailing flow regime.

The ratio of mass transfer coefficient to bubble size,  $k_L / d_B$ , calculated from measured  $k_L a_L$  and gas holdup via eq. (9), was found to remain constant for any given fluid, reactor, or the operating regime and gas flow rate (Fig. 14). This implies that  $k_L$  was directly proportional to the bubble size. In the two reactors used in our work there were no signifi-

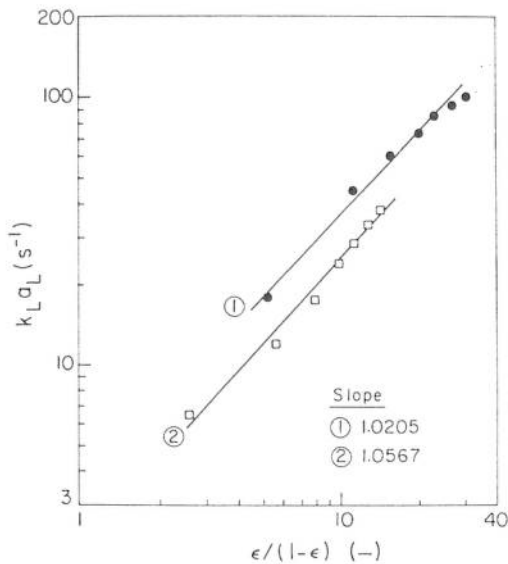


Figure 13.  $k_L a_L$  vs.  $\epsilon/(1 - \epsilon)$  in the airlift reactor. See Figure 4 for an explanation of the symbols.

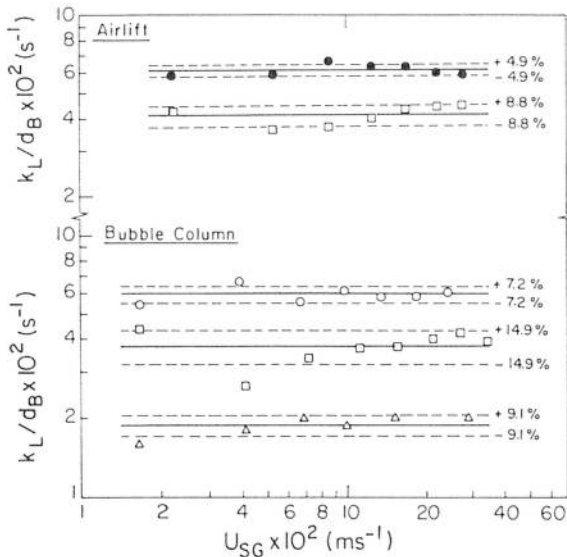


Figure 14. Mass transfer coefficient to bubble diameter ratio vs. the superficial gas velocity. The percentages refer to one standard deviation about the mean. See Figure 4 for an explanation of the symbols.

cant differences between the  $k_L/d_B$  values obtained in any one fluid, but this ratio depended strongly on the solid contents of the fluids and declined with increasing solid concentration (Fig. 15). The influence of solids on  $k_L/d_B$  ratio was described by the empirical equation:

$$-\ln\left(\frac{k_L}{d_B}\right) = 0.131C_2 + 2.772 \quad (15)$$

which applied to a large amount of data (ca. 94 results) within 5%. The obvious conclusion from this observation is that for bubbles of equal sizes in various fluids, the bubbles in the fluid containing a greater amount of suspended solids have lower mass transfer coefficient,  $k_L$ . This may be explained either in terms of the film theory as being due to

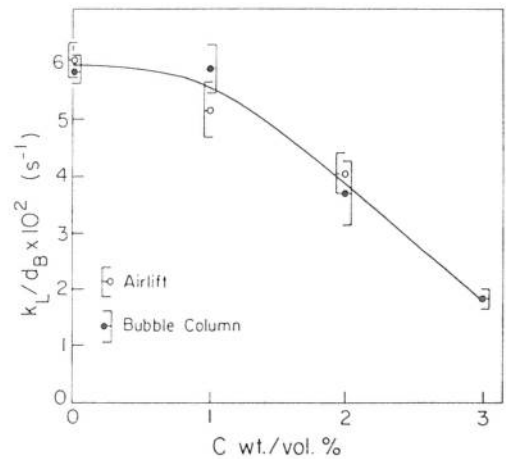


Figure 15. Influence of Solka Floc concentration in 0.15M NaCl on  $k_L/d_B$ . The vertical bars indicate the spread of results.

thicker films resulting from damped turbulence, or in terms of a reduced rate of surface renewal due again to the calming effect of solids close to the interface. Another explanation is possible: because there is no mass transfer through solids, the presence of solids on the interface may reduce the effective mass transfer area. Both these effects may contribute to  $k_L a_L$  reduction and the relative magnitude of each at present remains a matter of speculation.

The recommended correlations are for perforated-plate type for perforated-pipe-type spargers and may not apply to porous plate-sparged reactors, since for the latter the bubble size at birth is smaller than the expected equilibrium bubble size in dispersion.

## CONCLUSIONS

In suspensions which closely simulated mould fermentation media, increasing solid contents had a strong negative effect on gas holdup and  $k_L a_L$ . The bubble column performed better with respect to these parameters than the airlift under otherwise similar conditions. However, the potential positive effects of better mixing and circulation of loop-type pneumatic bioreactor devices should be noted.

For a given fluid in pneumatic reactors, the  $k_L/d_B$  ratio was more or less independent both of the reactor type and of the gas velocity. However, this ratio was very sensitive to the amount of solid in suspension and declined with increasing concentration of solids. These results indicate that attempts to improve  $k_L a_L$  in pneumatic reactors should focus on enhancement of gas holdup. The mass transfer coefficient,  $k_L$ , apparently declines with increasing amounts of solids.

This work was supported by a research grant from the National Science and Engineering Research Council of Canada. The assistance of Grant Allen with some of the measurements given in Table II is greatly appreciated.

## NOMENCLATURE

$a_L$  gas-liquid interfacial area per unit liquid volume ( $m^{-1}$ )  
 $B$  reciprocal of  $k_L a_L(s)$

$C$	concentration of solids [% (w/v) (dry wt)]
CMC	carboxymethyl cellulose
$C^*$	saturation concentration of oxygen in liquid (kg/m <sup>3</sup> )
$C_L$	concentration of oxygen in liquid (kg/m <sup>3</sup> )
$C_0$	initial concentration of oxygen in liquid (kg/m <sup>3</sup> )
$d_B$	sauter mean bubble diameter (m)
$d_c$	equivalent diameter of bubble column or airlift riser ( $=4 \times$ flow area/wetted perimeter) (m)
Fr	Froude number (dimensionless)
$g$	gravitational acceleration (m/s <sup>2</sup> )
$K$	consistency index (Pa s <sup><math>n</math></sup> )
$k_L$	mass transfer coefficient (m/s)
$n$	flow behavior index (dimensionless)
$Q_G$	volume flow rate of gas (m <sup>3</sup> /s)
$S$	electrode time delay (s)
SF	Solka Flocc
$t$	time
$t_G$	residence time of gas in liquid (s)
$U_{sg}$	superficial gas velocity based either on the bubble column cross section or on the riser cross section in the airlift (m/s)
$V_L$	liquid volume in reactor (m <sup>3</sup> )

#### Greek symbols

$\alpha$	constant in eq. (10) (dimensionless)
$\beta$	exponent in equation (10) (dimensionless)
$\epsilon$	volume fraction of gas in gas-liquid dispersion (dimensionless)

#### Subscripts

1	bubble flow
2	churn-turbulent flow

## References

1. H. Buchholz, R. Buchholz, J. Lücke, and K. Schügerl, *Chem. Eng. Sci.*, **33**, 1061 (1978).
2. H. J. Henzler, *Chem. Ing. Technol.*, **53**, 634 (1980).
3. M. Nakanoh and F. Yoshida, *Ind. Eng. Chem. Process Des. Dev.*, **19**, 190 (1980).
4. W.-D. Deckwer, K. Nguyen-Tien, A. Schumpe, and Y. Serpemen, *Biotechnol. Bioeng.*, **24**, 461 (1982).
5. S. P. Godbole, A. Schumpe, Y. T. Shah, and N. L. Carr, *AIChE J.*, **30**, 213 (1984).
6. B. G. Kelkar and Y. T. Shah, *AIChE J.*, **31**, 700 (1985).
7. Popovic, M., and Robinson, C. W., Proceedings of the 34th Canadian Chemical Engineering Congress, Quebec City, Quebec, Canada, 1984, p. 258.
8. J. Stejskal and F. Potuček, *Biotechnol. Bioeng.*, **27**, 503 (1985).
9. M. Reuss, D. Debus, and G. Zoll, *Chem. Eng.*, **XX**, 233 (June 1982).
10. S. A. El-Temtamy, S. A. Khalil, A. A. Nour-El-Din, and A. Gaber, *Appl. Microbiol. Biotechnol.*, **19**, 376 (1984).
11. K. Akita and F. Yoshida, *Ind. Eng. Chem. Process Des. Dev.*, **13**, 84 (1974).
12. M. Kawagoe, K. Nakao, and T. Otake, *J. Chem. Eng. Jpn.*, **8**, 254 (1975).
13. G. A. Hughmark, *Ind. Eng. Chem. Process Des. Dev.*, **6**, 218 (1967).
14. Miller, D. N., *AIChE J.*, **29**, 312 (1983).
15. Y. T. Shah, B. G. Kelkar, S. P. Godbole, and W.-D. Deckwer, *AIChE J.*, **28**, 353 (1982).